applied sciences

MDPI

Article

Sliding Mode Path following and Control Allocation of a Tilt-Rotor Quadcopter

Chih-Chen Yih * and Shih-Jeh Wu

Department of Mechanical & Automation Engineering, I-Shou University, Kaohsiung 84001, Taiwan
* Correspondence: ccyih@isu.edu.tw; Tel.: +886-7-657-7711 (ext. 3229)

Abstract: A tilt-rotor quadcopter (TRQ) equipped with four tilt-rotors is more agile than its under-actuated counterpart and can fly at any path while maintaining the desired attitude. To take advantage of this additional control capability and enhance the quadrotor system's robustness and capability, we designed two sliding mode controls (SMCs): the typical SMC exploits the properties of the rotational dynamics, and the modified SMC avoids undesired chattering. Our simulation studies show that the proposed SMC scheme can follow the planned flight path and keep the desired attitude in the presence of variable deviations and external perturbations. We demonstrate from the Lyapunov stability theorem that the proposed control scheme can guarantee the asymptotic stability of the TRQ in terms of position and attitude following via control allocation.

Keywords: tilt-rotor quadcopter (TRQ); sliding mode control (SMC); control allocation; path following

Citation: Yih, C.-C.; Wu, S.-J. Sliding Mode Path following and Control Allocation of a Tilt-Rotor Quadcopter. *Appl. Sci.* **2022**, *12*, 11088. https://doi.org/10.3390/app122111088

Academic Editors: Jaroslaw Pytka, Andrzej Łukaszewicz, Zbigniew Kulesza, Wojciech Giernacki and Andriy Holovatyy

Received: 27 September 2022
Accepted: 30 October 2022
Published: 1 November 2022

1. Introduction

Due to advancements in microprocessors and sensors, quadrotors have recently received much attention, playing an increasingly important role in unmanned aerial vehicles (UAVs). Now, quadrotors can easily hover indoors or outdoors and fly fast with global positioning system (GPS) devices or tiny cameras. Generally, changing the velocities of rotors [1,2] can generate lift and steering torque to control the attitude and position of the quadcopter.

Scholars and engineers have proposed several methods to solve the control problem for a quadrotor. These methods can be divided into: PID control [3–5], feedback linearization [6], optimal control [7], back-stepping [8,9], SMC [10–13], robust control [14], neural control [15,16], and nonlinear control [17]. To handle uncertainty systematically, researchers have extensively applied SMCs to address the robust control problem of quadrotors.

The super-twist control algorithm [18–20], a second-order SMC, has been studied to alleviate harmful chattering and maintain the robust capability of first-order SMCs. The studies in [21–23] demonstrate the stability and finite-time convergence of the super-twist control algorithm for single-variable systems through a Lyapunov stability analysis. For instance, Xu et al. [11] studied an adaptive terminal sliding mode for a quadrotor attitude control with specified capability and input saturation. In addition, Besnard et al. [12] proposed an observer-based SMC to address model uncertainty and wind perturbation. The recent work in [24,25] introduced the perturbation observer incorporating enhanced SMC for application in quadrotor UAV control.

Recently, several control methods have been proposed to solve the localization or following problem of under-actuated quadrotors, but these methods are still insufficient and have many shortcomings. For example, if the actuator fails or the rotor is damaged, the quadrotor will crash due to a lack of actuator redundancy to restore attitude and position. Tilt-rotor quadrotors [26] can increase the degree of control freedom and provide control redundancy. Compared with under-actuated quadrotors, full-drive quadrotors have more flexibility than under-actuated quadrotors and have recently attracted the research community's attention. Ryll et al. [27] proposed a modeling approach for an

overdrive quadrotor UAV. They provide a dynamic linearization control that uses higher-order derivatives of the measured output. Hua et al. [28] studied the control of vertical take-off and landing (VTOL) vehicles with bank thrust angle limitation. The proposed control can achieve the primary and secondary goals of asymptotically stabilizing position and direction. Recently, Rashad et al. [29] reviewed various UAV designs with fully actuated multi-rotors, in the literature. They introduced the control allocation matrix to categorize the proposed hardware framework and discussed the criteria for optimizing the UAV design. Zheng et al. [30] introduced the hardware design of an experimental tilt-rotor drone that uses linear servo motors to control the tilt mechanism. The authors also implemented and tested their PD-based translation and attitude control scheme on the fully actuated prototype quadrotor. To control the hovering and fixed-wing flight of a tilt-rotor UAV and the transition between them, Willis et al. [31] proposed a control scheme, which includes a low-level angular rate controller and a variable mixer, and an LQR following control

We propose a TRQ model based on translational and rotational dynamics, perturbation, and model uncertainty. Note that the SMC presented for an under-actuated quadrotor cannot be directly applied to a tilt-rotor quadrotor. We propose an SMC scheme with control allocation, exploiting the structural features of rotational dynamics and avoiding chattering in translational dynamics to further enhance the robustness and capability of TRQ systems.

The paper is organized as follows: Section 2 discusses the TRQ's dynamics and various drive modes. Section 3 presents the proposed SMC scheme and control assignment. Section 4 provides a stability analysis. In Section 5, the proposed SMC scheme is applied to a TRQ for numerical simulation. Section 6 gives some conclusions.

2. Dynamic Model of a Tilt-Rotor Quadcopter (TRQ) with Various Actuation Modes

This section will establish a dynamic model from the Newton–Euler equation. First, we present the dynamics of the TRQ (Figure 1). Using the variables defined in the nomenclature, we propose various actuation modes from over-actuated, to fully actuated, to under-actuated modes.

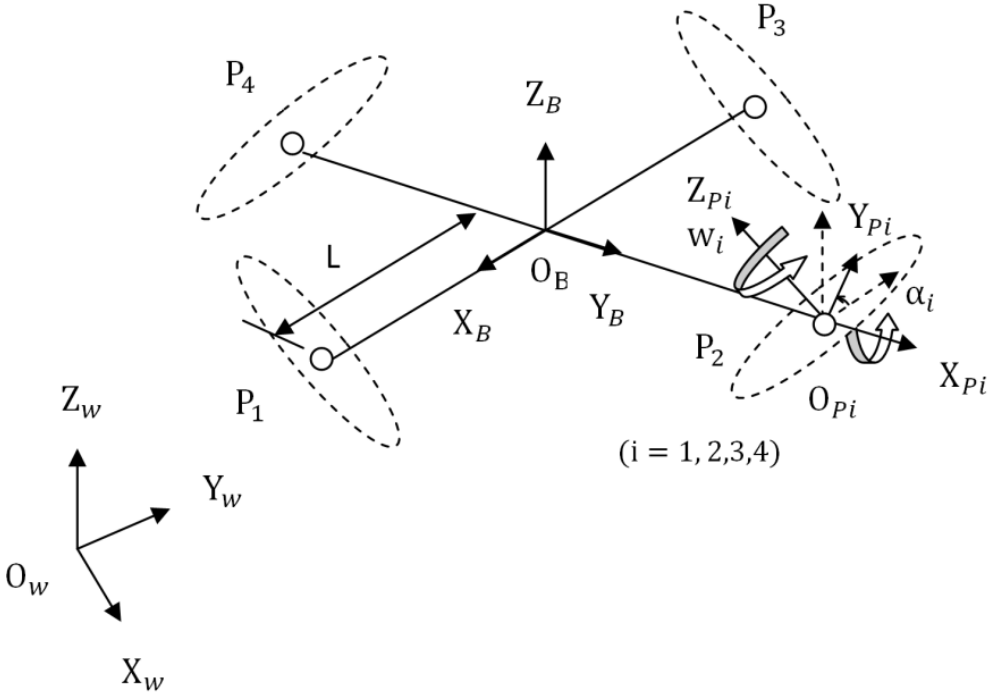

Figure 1. The schematic diagram of the TRQ for modeling.

2.1. Rotational and Translational Dynamics

The rotation matrix ${}^{B}R_{P_i}$ from the ith rotor frame to the body frame is

$$ {}^{B}R_{P_i} = R_Z(\beta_i)R_X(\alpha_i) \tag{1}$$

$$R_X(\alpha_i) = \begin{bmatrix} 1 & 0 & 0 \\ 0 & \cos\alpha_i & -\sin\alpha_i \\ 0 & \sin\alpha_i & \cos\alpha_i \end{bmatrix},$$

and

$$R_Z(\beta_i) = \begin{bmatrix} \cos\beta_i & -\sin\beta_i & 0 \\ \sin\beta_i & \cos\beta_i & 0 \\ 0 & 0 & 1 \end{bmatrix},\ \beta_i = (i-1)\frac{\pi}{2},\ i = 1,\ 2,\ 3,\ 4.$$

The angular velocity is

$$w_{Pi} = {}^{P_i}R_B w_B + \begin{bmatrix} \dot{\alpha}_i & 0 & w_i \end{bmatrix}^T \tag{2}$$

We define

$$sgn(x) = \begin{cases} 1 & if\ \ x > 0 \\ -1 & if\ \ x < 0 \end{cases}$$

where

$$w_1 < 0,\ w_3 < 0\ ,\ w_2 > 0,\ w_4 > 0$$

The rotational dynamics of the TRQ can be formulated as:

$$\tau_B = I_B\dot{w}_B + w_B \times I_B w_B + \sum_{i=1}^{4} {}^{B}R_{P_i}\tau_{Pi} \tag{3}$$

where

$$\tau_{Pi} = I_{Pi}\dot{w}_{Pi} + w_{Pi} \times I_{Pi}w_{Pi} - \tau_{di} \tag{4}$$

$$\tau_{di} = \begin{bmatrix} 0 & 0 & -k_m w_i^2 sgn(w_i) \end{bmatrix}^T \tag{5}$$

The force in the rotor frame is

$$T_{pi} = \begin{bmatrix} 0 & 0 & k_f w_i^2 \end{bmatrix}^T \tag{6}$$

and the toque in body frame is

$$\tau_B = \sum_{i=1}^{4} ({}^{B}O_{P_i} \times {}^{B}R_{P_i}T_{Pi}) \tag{7}$$

The transform between body angular rates to the Euler rates is

$$\dot{r} = R_T w_B \tag{8}$$

where

$$R_T = \begin{bmatrix} 1 & s_\phi \tan\theta & c_\phi \tan\theta \\ 0 & c_\phi & -s_\phi \\ 0 & s_\phi \sec\theta & c_\phi \sec\theta \end{bmatrix} \tag{9}$$

and $r = \begin{bmatrix} \phi & \theta & \psi \end{bmatrix}^T \in R^3$ is the attitude vector of the roll, the pitch, and the yaw angle. We denote $s_{q_i} = \sin q_i$ and $c_{q_i} = \cos\ q_i$.

Taking the derivative of (8) and ignoring I_{Pi} in (4), we have

$$\ddot{r} = \dot{R}_T R_T^{-1}\dot{r} + R_T I_B^{-1}(\tau_B - w_B \times I_B w_B + \sum_{i=1}^{4} {}^{B}R_{P_i}\tau_{di}) \tag{10}$$

We denote

$$\tau = \sum_{i=1}^{4} ({}^{B}O_{P_i} \times {}^{B}R_{P_i} T_{Pi}) + \sum_{i=1}^{4} {}^{B}R_{P_i} \tau_{di} \tag{11}$$

Define the transform matrix

$$\Psi = R_T^{-1} \tag{12}$$

From (8), we have

$$w_B = \Psi \dot{r} \tag{13}$$

It follows from (10) and (12) that

$$\begin{aligned} \Psi^T I_B \Psi \ddot{r} &= -\Psi^T I_B \dot{\Psi} \dot{r} - \Psi^T w_B \times I_B w_B + \Psi^T \tau \\ &= -\left[\Psi^T I_B \dot{\Psi} + \Psi^T (\Psi \dot{r} \times I_B \Psi)\right] \dot{r} + \Psi^T \tau \end{aligned} \tag{14}$$

Considering the perturbation torque τ_d, we obtain

$$H(r)\ddot{r} + C(r, \dot{r})\dot{r} = \Psi^T(\tau + \tau_d) \tag{15}$$

where

$$H(r) = \Psi^T I_B \Psi \tag{16}$$

$$C(r, \dot{r}) = \left[\Psi^T I_B \dot{\Psi} + \Psi^T (\Psi \dot{r} \times I_B \Psi)\right] \tag{17}$$

$$\Psi(r) = \begin{bmatrix} 1 & 0 & -s_\theta \\ 0 & c_\phi & c_\theta s_\phi \\ 0 & -s_\phi & c_\theta c_\phi \end{bmatrix} \tag{18}$$

and $H(r) \in R^{3\times 3}$ is the inertia matrix, $C(r, \dot{r})\dot{r} \in R^3$ represents the centrifugal and Coriolis forces. $\tau = \begin{bmatrix} \tau_\phi & \tau_\theta & \tau_\psi \end{bmatrix}^T \in R^3$ is the vector of torques and $\tau_d \in R^3$ is the perturbation torque.

The velocity in F_w is

$$\dot{p} = {}^{W}R_B V_B \tag{19}$$

The derivative of velocity in F_B can be expressed as

$$\dot{V}_B = -w_B \times V_B + {}^{W}R_B^T \begin{bmatrix} 0 & 0 & -g \end{bmatrix}^T + \frac{f}{m} \tag{20}$$

where

$${}^{W}R_B = \begin{bmatrix} c_\theta c_\psi & s_\phi s_\theta c_\psi - c_\phi s_\psi & c_\phi s_\theta c_\psi + s_\phi s_\psi \\ c_\theta s_\psi & s_\phi s_\theta s_\psi + c_\phi c_\psi & c_\phi s_\theta s_\psi - s_\phi c_\psi \\ -s_\theta & s_\phi c_\theta & c_\phi c_\theta \end{bmatrix}$$

and

$$f = \sum_{i=1}^{4} {}^{B}R_{P_i} T_{Pi} \tag{21}$$

where $p = \begin{bmatrix} x & y & z \end{bmatrix}^T \in R^3$. $f = \begin{bmatrix} f_x & f_y & f_z \end{bmatrix}^T \in R^3$ is the vector of forces.

Taking the derivative of (19), ignoring ${}^{W}\dot{R}_B$ and using (20), the translational dynamics becomes

$$m\ddot{p} = {}^{W}R_B = (-w_B \times V_B + f) - \begin{bmatrix} 0 & 0 & mg \end{bmatrix}^T + u_d \tag{22}$$

where $u_d \in R^3$ is the perturbation force in F_w.

2.2. Over-Actuated, Fully Actuated, and Under-Actuated Modes

Denote $\alpha = [\alpha_1 \quad \alpha_2 \quad \alpha_3 \quad \alpha_4]^T$,$w = [w_1 \quad w_2 \quad w_3 \quad w_4]^T$, $s_i = \sin\alpha_i$, and $c_i = \cos\alpha_i$, one can arrange (21) and (11) as

$$\begin{bmatrix} f \\ \tau \end{bmatrix} = \begin{bmatrix} K_1(\alpha) \\ K_2(\alpha) \end{bmatrix} U(w) \tag{23}$$

where

$$U = \begin{bmatrix} w_1^2 & w_2^2 & w_3^2 & w_4^2 \end{bmatrix}^T$$

$$K_1(\alpha) = \begin{bmatrix} 0 & k_f s_2 & 0 & -k_f s_4 \\ -k_f s_1 & 0 & k_f s_3 & 0 \\ k_f c_1 & k_f c_2 & k_f c_3 & k_f c_4 \end{bmatrix} \tag{24}$$

$$K_2(\alpha) = \begin{bmatrix} 0 & Lk_f c_2 - k_m s_2 & 0 & -Lk_f c_4 + k_m s_4 \\ -Lk_f s_1 - k_m s_1 & 0 & Lk_f c_3 + k_m s_3 & 0 \\ -Lk_f s_1 + k_m c_1 & -Lk_f s_2 - k_m c_2 & -Lk_f s_3 + k_m s_3 & -Lk_f s_4 - k_m s_4 \end{bmatrix} \tag{25}$$

Remark 1. *Over-actuated and fully actuated modes.*

For over-actuated mode, the vector of tilt angles is

$$\alpha = [\alpha_1 \quad \alpha_2 \quad \alpha_3 \quad \alpha_4]^T$$

By setting $\alpha_3 = -\alpha_1$, $\alpha_4 = -\alpha_2$, the vector of tilt angles for fully actuated mode is

$$\alpha = [\alpha_1 \quad \alpha_2 \quad \alpha_1 \quad \alpha_2]^T$$

Remark 1. *Under-actuated mode.*

By setting $\alpha = \begin{bmatrix} 0 & 0 & 0 & 0 \end{bmatrix}^T$, the force and the torque in (23) for the under-actuated mode can be reduced as

$$\begin{bmatrix} f_z \\ \tau_\phi \\ \tau_\theta \\ \tau_\psi \end{bmatrix} = \begin{bmatrix} k_f & k_f & k_f & k_f \\ 0 & Lk_f & 0 & -Lk_f \\ -Lk_f & 0 & Lk_f & 0 \\ k_m & -k_m & k_m & -k_m \end{bmatrix} U(w) \tag{26}$$

3. Sliding Mode Path following and Control Allocation

In this section, we first propose the sliding mode-based attitude and position following control via torque and force in (23). Then, we present the control allocation from the control torque and force to the speed and tilt angle of four rotors. Figure 2 illustrates the TRQ control scheme.

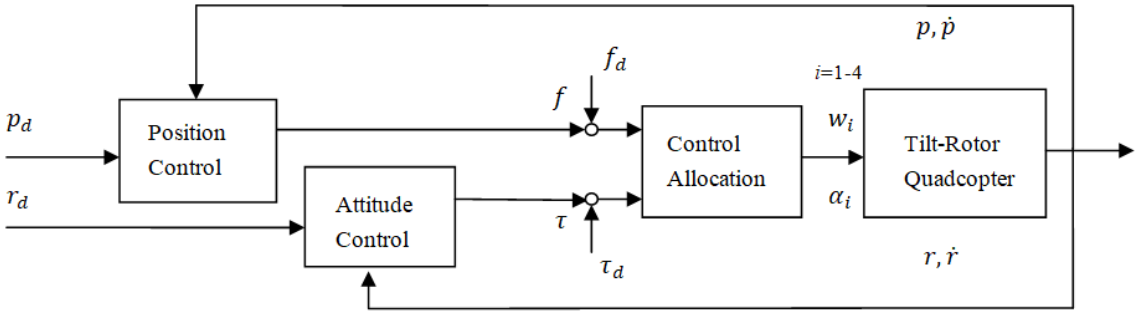

Figure 2. The TRQ control scheme.

3.1. Attitude and Position following SMC

Define $s_1 \in R^3$

$$\dot{r}_r = \dot{r}_d - \Lambda_1(r - r_d) \tag{27}$$

and

$$s_1 = \dot{r} - \dot{r}_r = \dot{r} - \dot{r}_d + \Lambda_1(r - r_d) \tag{28}$$

where r_d is the desired attitude and $\dot{r}_d$ is the desired angular velocity.

Now, we propose the following control for attitude following to exploit the structure of the rotational dynamics:

$$\tau = \Psi^{-T}\left[\hat{H}\ddot{r}_r + \hat{C}\dot{r}_r - K_1\, SGN(s_1) - K_3 s_1 - K_4\tilde{r}\right] \tag{29}$$

where $\tilde{r} = r - r_d$ and $\widehat{(\cdot)}$ denotes the nominal of $(\cdot)$. K_1, K_3, K_4 are positive diagonal matrices, $sgn(\cdot)$ is the sign function, and

$$SGN\left([x_1 \;\; x_2 \;\; x_3]^T\right) = [sgn(x_1) \;\; sgn(x_2) \;\; sgn(x_3)]^T \tag{30}$$

We can now define $s_2 \in R^3$

$$s_2 = \dot{p} - \dot{p}_d + \Lambda_2(p - p_d) \tag{31}$$

where p_d is the desired position and $\dot{p}_d$ is the desired velocity.

The position following control is proposed to alleviate the chattering effects as follows:

$$f = {}^{W}R_B^{-1}\left(u + \begin{bmatrix} 0 \\ 0 \\ mg \end{bmatrix}\right) \tag{32}$$

where u is designed as follows:

$$\dot{u} = -(K_2 + \Lambda_2)u + \hat{m}\left((K_2 + \Lambda_2)\ddot{p}_d + \dddot{p}_d - K_2\Lambda_2(\dot{p} - \dot{p}_d) - \Lambda_3 s_2 - \Lambda_4\, SGN(s_2)\right) \tag{33}$$

where K_2, Λ_2, Λ_3, Λ_4 are positive diagonal matrices.

3.2. Control Allocation

3.2.1. Fully Actuated Mode

We use the following assumption for the fully actuated quadcopter system

$$\alpha_3 = -\alpha_1, \quad \alpha_4 = -\alpha_2 \tag{34}$$

Now, we propose the following steps to compute α_i and w_i:

Step 1: Initially, set the tilt angles ($\alpha_1 = \alpha_2 = 0$).

Step 2: Compute f and τ from (32) and (29).

Step 3: Compute the rotor velocities.

$$\begin{bmatrix} w_1^2 \\ w_2^2 \\ w_3^2 \\ w_4^2 \end{bmatrix} = \begin{bmatrix} k_f c_1 & k_f c_2 & k_f c_3 & k_f c_4 \\ 0 & Lk_f c_2 - k_m s_2 & 0 & -Lk_f c_4 + k_m s_4 \\ -Lk_f c_1 - k_m s_1 & 0 & Lk_f c_3 + k_m s_3 & 0 \\ -Lk_f s_1 + k_m c_1 & -Lk_f s_2 - k_m c_2 & -Lk_f s_3 + k_m c_3 & -Lk_f s_4 - k_m c_4 \end{bmatrix}^{-1} \begin{bmatrix} f_z \\ \tau_\phi \\ \tau_\theta \\ \tau_\psi \end{bmatrix} \tag{35}$$

where $s_i = \sin\alpha_i$ and $c_i = \cos\alpha_i$ $(i = 1,\ 2,\ 3,\ 4)$.

Step 4: Compute the tilt angles from (23) and (24) using (34) as follows:

$$\alpha_1 = \sin^{-1}\left(\frac{-f_y}{k_f(w_1^2 + w_3^2)}\right) = -\alpha_3 \tag{36}$$

$$\alpha_2 = \sin^{-1}\left(\frac{f_x}{k_f\left(w_2^2 + w_4^2\right)}\right) = -\alpha_4 \tag{37}$$

Step 5: Go to Step 2 to continue the iteration.

3.2.2. Over-Actuated Mode

We propose the steps to compute α_i and w_i:
Step 1: Initially, set the tilt angles $\alpha_i = 0$ ($i = 1, 2, 3, 4$).
Step 2: Compute f and τ from (32) and (29).
Step 3: Compute the rotor velocities from (35).
Step 4: Compute the tilt angles from (23)–(25) as follows:

$$\left(k_f s_2\right) w_2^2 + \left(-k_f s_4\right) w_4^2 = \tau_\phi \tag{38}$$

$$\left(Lk_f c_2 - k_m s_2\right) w_2^2 + \left(-Lk_f c_4 + k_m s_4\right) w_4^2 = \tau_\phi \tag{39}$$

$$\left(-k_f s_1\right) w_1^2 + \left(k_f s_3\right) w_3^2 = \tau_\theta \tag{40}$$

$$\left(-Lk_f c_1 - k_m s_1\right) w_1^2 + \left(Lk_f c_3 + k_m s_3\right) w_3^2 = \tau_\theta \tag{41}$$

where $s_i = \sin\alpha_i$ and $c_i = \cos\alpha_i (i = 1,\ 2,\ 3,\ 4)$. Using the triangular identities $s_i^2 + c_i^2 = 1\ (i = 1,\ 2,\ 3,\ 4)$, one can use the numerical method to solve for α_i in the system of nonlinear equations.

Step 5: Go to Step 2 to continue the iteration.

3.2.3. Under-Actuated Mode

Notice that, due to the lack of control degrees of freedom, the desired attitude ϕ_d and θ_d is not arbitrary for the under-actuated quadrotor.

One can obtain ϕ_d and θ_d by

$$\phi_d = \sin^{-1}\left(\frac{u_x s_{\psi d} - u_y c_{\psi d}}{\sqrt{u_x^2 + u_y^2 + (u_z + mg)^2}}\right) \tag{42}$$

$$\theta_d = \tan^{-1}\left(\frac{u_x c_{\psi d} + u_y s_{\psi d}}{u_z + mg}\right) \tag{43}$$

The vector of w_i^2 is

$$\begin{bmatrix} w_1^2 \\ w_2^2 \\ w_3^2 \\ w_4^2 \end{bmatrix} = \begin{bmatrix} k_f & k_f & k_f & k_f \\ 0 & -Lk_f & 0 & Lk_f \\ -Lk_f & 0 & Lk_f & 0 \\ k_m & -k_m & k_m & -k_m \end{bmatrix}^{-1} \begin{bmatrix} f \\ \tau_\phi \\ \tau_\theta \\ \tau_\psi \end{bmatrix} \tag{44}$$

4. Stability Analysis

This section presents the stability analysis of the SMC scheme. Let us use $\lambda_M(A)$, $\lambda_m(A)$ for the largest and smallest eigenvalue of a matrix A. We denote the Euclidean norm for an $n \times 1$ vector x by $\|x\| = \sqrt{x^T x}$. The inertia matrix is symmetric, positive definite, and bounded by $0 < \lambda_m(H) \leq \|H(r)\| \leq \lambda_M(H)$. The matrix $\dot{H}(r) - 2C\left(r, \dot{r}\right)$ is skew-symmetric.

4.1. Sliding Mode Attitude following Control

Theorem 1. *Consider the dynamic model described in (15) and the control for attitude following in (29). The attitude following error dynamics is exponentially stable if the switching gain satisfies the following condition.*

$$\lambda_m(K_1) \geq \left(\|\widetilde{H}\| \|\ddot{r}_r\| + \|\widetilde{C}\| \|\dot{r}_r\| + \|\tau_d\| \right) + \varepsilon_1 \tag{45}$$

where ε_1 is a positive constant.

Proof. $\widehat{H}$ and $\hat{C}$ represent the nominal H and C, where $\widetilde{H} = H - \widehat{H}$ and $\widetilde{C} = C - \hat{C}$.

The rotational dynamics can be expressed as follows:

$$\widehat{H}(q)\ddot{r} + \hat{C}(r,\dot{r})\dot{q} = \Psi^T(\tau + \tau_d) + h_1(r,\dot{r},\ddot{r}) \tag{46}$$

$$h_1(r,\dot{r},\ddot{r}) = -\widetilde{H}(r)\ddot{r} - \widetilde{C}(r,\dot{r})\dot{r}$$

Define

$$\dot{r}_r = \dot{r}_d - \Lambda_1(r - r_d) \tag{47}$$

and

$$s_1 = \dot{r} - \dot{r}_r = \dot{r} - \dot{r}_d + \Lambda_1(r - r_d) \tag{48}$$

It follows from (48) that

$$\dot{s}_1 = \ddot{r} - \ddot{r}_r = \ddot{r} - \ddot{r}_d + \Lambda_1(\dot{r} - \dot{r}_d) \tag{49}$$

Now, we propose the control

$$\tau = \Psi^{-T}\left[\hat{H}\ddot{r}_r + \hat{C}\dot{r}_r - K_1\, SGN(s_1) - K_3 s_1 - K_4\tilde{r}\right] \tag{50}$$

where $\tilde{r} = r - r_d$ and $K_1,\ K_3,$ and K_4 are diagonal matrices. □

Define the Lyapunov function

$$V_1 = \frac{1}{2}s_1^T M(r)s_1 + \frac{1}{2}\tilde{r}^T K_4 \tilde{r} \tag{51}$$

Using (50) and taking derivative of V_1 yield

$$\dot{V}_1 = s_1^T H\dot{s}_1 + \frac{1}{2}s_1^T \dot{H}s_1 + \tilde{r}^T K_4 \dot{\tilde{r}} \tag{52}$$

If the switching gain meets the condition as follows

$$\lambda_m(K_1) \geq \left(\|\widetilde{H}\| \|\ddot{r}_r\| + \|\widetilde{C}\| \|\dot{r}_r\| + \|\tau_d\| \right) + \varepsilon_1 \tag{53}$$

where ε_1 is a positive constant.

From (52), we have

$$\dot{V}_1 \leq -\varepsilon_1\, s_1^T SGN(s_1) - s_1^T K_3 s_1 - \tilde{r}^T K_4 \tilde{r} < 0\ ,\ s_1 \neq 0 \tag{54}$$

The following adaptation law can replace the switching gain K_1

$$K_1 = diag([k_1\ \ k_2\ \ k_3]) \tag{55}$$

$$k_i(t) = k_{ci}|\eta_i| + k_{mi}$$

where $k_{ci} > 0$, $k_{mi} > 0$ and η_i is the obtained by filtering the $sgn(s_{1i})$ using a low-pass filter

$$\zeta_i \dot{\eta}_i + \eta_i = sgn(s_{1i}),\ \eta_i(0) = 0 \tag{56}$$

where ζ_i is a positive constant.

4.2. Sliding Mode Position following Control

Theorem 2. *Consider the translational dynamic model described in (21) and the control for position following in (32)–(33). The position following error dynamics is then asymptotically stable.*

Proof. The translational dynamics is

$$\ddot{p} = \frac{1}{m}u + \frac{u_d}{m} \tag{57}$$

where

$$u = \begin{bmatrix} u_x \\ u_y \\ u_z \end{bmatrix} = {}^{W}R_B f - \begin{bmatrix} 0 \\ 0 \\ mg \end{bmatrix} \tag{58}$$

The nominal dynamics is

$$\ddot{p} = \frac{1}{\widehat{m}}u + \frac{\hat{u}_d}{\widehat{m}} \tag{59}$$

where $\widehat{m}$ is the nominal mass and $\hat{u}_d = 0$.

The sliding surface $s_2 \in R^3$ is

$$s_2 = \dot{p} - \dot{p}_d + \Lambda_2(p - p_d) \tag{60}$$

Using (57) yields

$$\dot{s}_2 = \frac{1}{\widehat{m}}u - \ddot{p}_d + \Lambda_2(\dot{p} - \dot{p}_d) \tag{61}$$

and

$$\dot{s}_2 = \frac{1}{\widehat{m}}\dot{u} - \dddot{p}_d + \Lambda_2(\dot{s}_2 - \Lambda_2(\dot{p} - \dot{p}_d)\ ) \tag{62}$$

Define the Lyapunov function

$$V_2 = \frac{1}{2}s_2^T\Lambda_3 s_2 + \frac{1}{2}\dot{s}_2^T\dot{s}_2 + \gamma ABS(s_2) \tag{63}$$

where

$$\gamma = [\gamma_1\ \gamma_2\ \gamma_3]$$

It follows from (63) that

$$\dot{V}_2 = \dot{s}_2^T\left(\ddot{s}_2 + \Lambda_3 s_2 + \Lambda_4\ SGN(s_2)\right) \tag{64}$$

where Λ_4 is a diagonal matrix with diagonal elements $[\gamma_1\ \gamma_2\ \gamma_3]$.

Then

$$\ddot{s}_2 + \Lambda_3 s_2 + \Lambda_4\ SGN(s_2) = -K_2\dot{s}_2 \tag{65}$$

and

$$\dot{V}_2 = -K_2\dot{s}_2^T\dot{s}_2 \tag{66}$$

Using (62) and (65) yields

$$\dot{u} = \widehat{m}\left(-(K_2 + \Lambda_2)\dot{s}_2 - \Lambda_3 s_2 - \Lambda_4\ SGN(s_2) + \dddot{p}_d + \Lambda_2^2(\dot{p} - \dot{p}_d)\right) \tag{67}$$

Substituting $\dot{s}_2$ from (61) into (64), we have

$$\dot{u} = -(K_2 + \Lambda_2)u + \widehat{m}\big((K_2 + \Lambda_2)\ddot{p}_d + \dddot{p}_d - K_2\Lambda_2(\dot{p} - \dot{p}_d) - \Lambda_3 s_2 - \Lambda_4\, SGN(s_2)\big) \quad (68)$$

We can derive from LaSalle-Yoshizawa theorem and (66) that $\dot{s}_2 \to 0$. On the basis of (62) and the Barbalat's lemma, one can conclude that $\ddot{s}_2 \to 0$. Therefore, we have the following from (65)

$$\Lambda_3 s_2 = -\Lambda_4\, SGN(s_2) \quad (69)$$

which ensures that

$$s_2 = 0 \quad (70)$$

□

5. Numerical Simulation

To illustrate the proposed control scheme's design, we give an example of a fully actuated TRQ.

5.1. Simulation Parameters

Assuming $s_{q_i} = \sin q_i,\ c_{q_i} = \cos q_i,$ we have

$$H_{11} = I_x, H_{12} = 0,\ H_{13} = -I_x s_\theta$$
$$H_{22} = I_y c_\phi^2 + I_z s_\phi^2,\ H_{23} = c_\theta c_\phi s_\phi (I_y - I_z)$$
$$H_{33} = I_x s_\theta^2 + I_y c_\theta^2 s_\phi^2 + I_z c_\theta^2 c_\phi^2$$

The matrix of $C(r, \dot{r})$ is

$$C_{11} = 0$$
$$C_{12} = -I_x \dot{\psi} c_\theta + (I_y - I_z)\left(\dot{\theta} s_\phi c_\phi + \dot{\psi} c_\theta s_\phi^2 - \dot{\psi} c_\theta c_\phi^2\right)$$
$$C_{13} = -I_y \dot{\psi} c_\theta^2 s_\phi c_\phi + I_z \dot{\psi} c_\theta^2 s_\phi c_\phi$$
$$C_{21} = I_x \dot{\psi} c_\theta - (I_y - I_z)\left(\dot{\theta} s_\phi c_\phi + \dot{\psi} c_\theta s_\phi^2 - \dot{\psi} c_\theta c_\phi^2\right)$$
$$C_{22} = -I_y \dot{\phi} s_\phi c_\phi + I_z \dot{\phi} s_\phi c_\phi$$
$$C_{23} = -I_x \dot{\psi} s_\theta c_\theta + I_y \dot{\psi} s_\theta c_\theta s_\phi^2 + I_z \dot{\psi} s_\theta c_\theta c_\phi^2$$
$$C_{31} = -I_x \dot{\theta} c_\theta + I_y \dot{\psi} c_\theta^2 s_\phi c_\phi - I_z \dot{\psi} c_\theta^2 s_\phi c_\phi$$
$$C_{32} = I_x \dot{\psi} s_\theta c_\theta + (I_z - I_y)\left(\dot{\theta} s_\theta s_\phi c_\phi + \dot{\phi} c_\theta s_\phi^2 - \dot{\phi} c_\theta c_\phi^2\right) - I_y \dot{\psi} s_\theta c_\theta s_\phi^2 - I_z \dot{\psi} s_\theta c_\theta c_\phi^2$$
$$C_{32} = I_x \dot{\psi} s_\theta c_\theta + (I_z - I_y)\left(\dot{\theta} s_\theta s_\phi c_\phi + \dot{\phi} c_\theta s_\phi^2 - \dot{\phi} c_\theta c_\phi^2\right) - I_y \dot{\psi} s_\theta c_\theta s_\phi^2 - I_z \dot{\psi} s_\theta c_\theta c_\phi^2$$
$$C_{33} = I_x \dot{\theta} s_\theta c_\theta + I_y\left(-\dot{\theta} s_\theta c_\theta s_\phi^2 + \dot{\phi} c_\theta^2 s_\phi c_\phi\right) - I_z\left(\dot{\theta} s_\theta c_\theta c_\phi^2 + \dot{\phi} c_\theta^2 s_\phi c_\phi\right)$$

We employ the following variables for simulation:

$$m = 2\text{kg},\ L = 0.275\text{m}, g = 9.81\text{m/s}^2,$$
$$I_x = 0.025\text{kgm}^2,\ I_y = 0.025\text{kgm}^2, I_z = 0.040\text{kgm}^2,$$
$$k_m = 2.67{\cdot}10^{-7}\text{Ns}^2,\ k_f = 1.5{\cdot}10^{-5}\text{Nms}^2.$$

with initial conditions

$$\begin{bmatrix} x(0) & y(0) & z(0) \end{bmatrix} = \begin{bmatrix} 0 & 0 & 0 \end{bmatrix}$$

and the desired positions

$$\begin{bmatrix} x_d(t_f) & y_d(t_f) & z_d(t_f) \end{bmatrix} = \begin{bmatrix} 20 & 10 & 5 \end{bmatrix}$$

where $t_f = 20$. The desired attitudes are

$$\phi_d = 0,\ \theta_d = 0,\ \psi_d = 0$$

The desired path is defined as

$$\begin{aligned} x_d(t) &= 2.5{\cdot}10^{-2}\ t^3 - 1.875{\cdot}10^{-3}\ t^4 + 3.75{\cdot}10^{-5}\ t^5 \\ y_d(t) &= 1.25{\cdot}10^{-2}\ t^3 - 9.375{\cdot}10^{-4}\ t^4 + 1.875{\cdot}10^{-5}\ t^5 \\ z_d(t) &= 6.25{\cdot}10^{-3}\ t^3 - 4.6875{\cdot}10^{-4}\ t^4 + 9.375{\cdot}10^{-6}\ t^5 \end{aligned}$$

Now, we use the following control parameters for simulation:

$$\begin{aligned} &\Lambda_1 = 10\ I_2\ , \Lambda_2 = 4I_3,\ \Lambda_3 = 40\ I_3,\ \Lambda_4 = I_3, K_1 = I_3, \\ &K_2 = 4I_3, K_3 = 4I_3, K_4 = 10I_3, k_{ci} = 4I_3,\ \ k_{mi} = 0.1I_3,\ \ (i = 1,2,3). \end{aligned}$$

5.2. Simulation Results

We present the simulation results of the proposed attitude and position following SMC control in Figures 3–8. Figures 3 and 4 show the attitude and position trajectories of the quadrotor with variable changes (weights increased to 125%). The simulation results in Figures 3 and 4 show that the proposed SMC can successfully drive the quadrotor from the initial position through the desired path to the final destination while maintaining the desired attitude. Figures 5 and 6 show the lift and steering torque produced by the four tilt-rotors of the TRQ. Figure 7 shows the path of the tilt angle with parameter deviation. The corresponding quadrotor speeds are shown in Figure 8.

Because the stability analysis in the previous section demonstrated robustness with respect to parameter uncertainty and external perturbations, we then further evaluated the impact of external perturbations on the TRQ. We used perturbation force [sin(4t) − sin(4t) 2sin(4t)] N and perturbation torque [0.1sin(2t) 0.1sin(2t) 0.1sin(2t)] Nm applied to TRQ for simulated motion. As shown in Figures 9–14, we can see that the perturbation has little effect on the capability of the quadcopter because the proposed control and control assignment can reject the perturbation and return the state variables to the sliding surface.

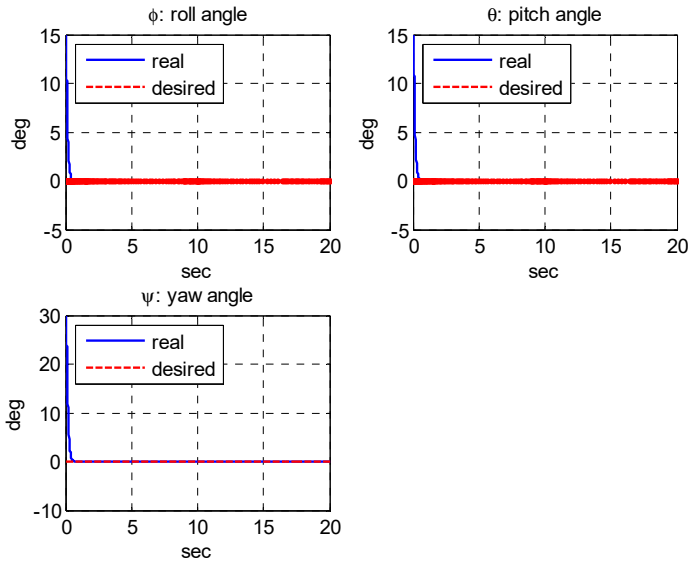

Figure 3. The attitude path with variable deviations.

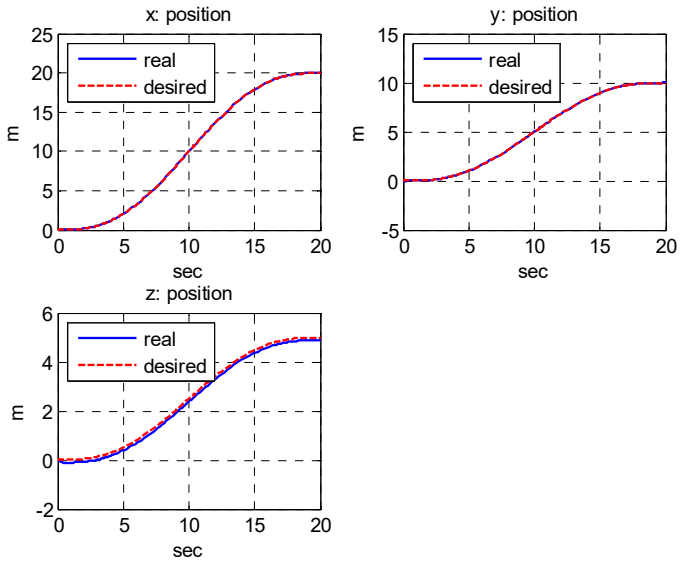

Figure 4. The position path with variable deviations.

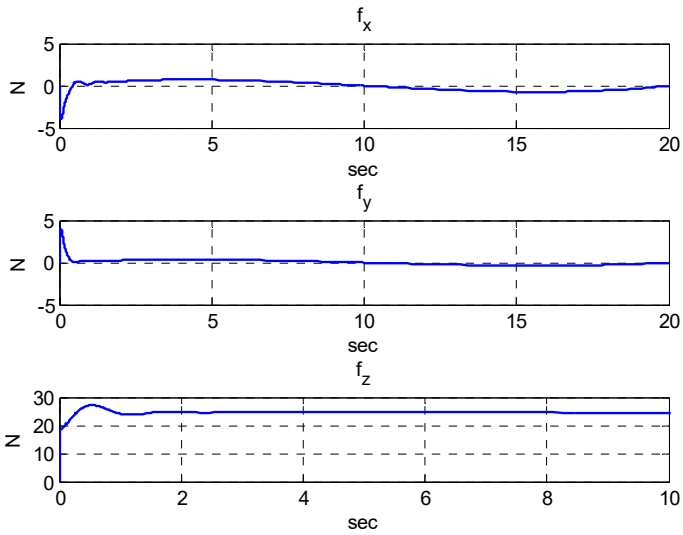

Figure 5. The propelling force with variable deviations.

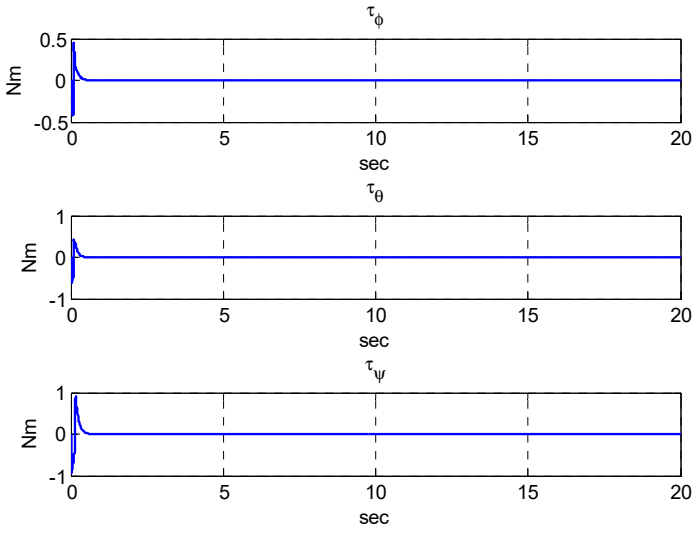

Figure 6. The turning torque with variable deviations.

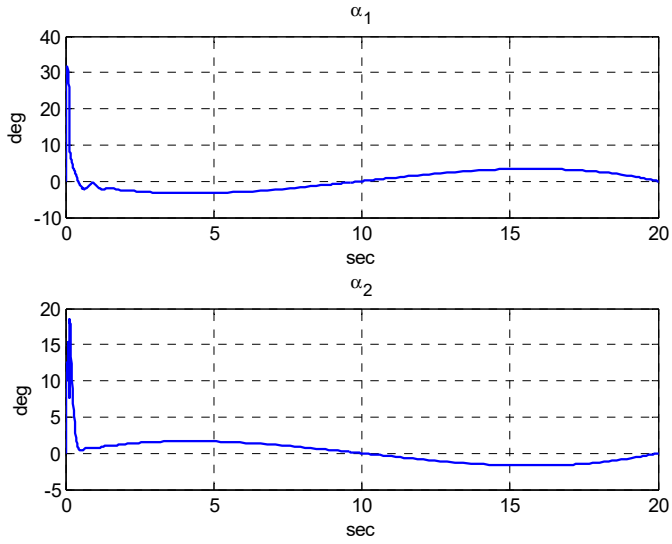

Figure 7. The tilt angle path with variable deviations.

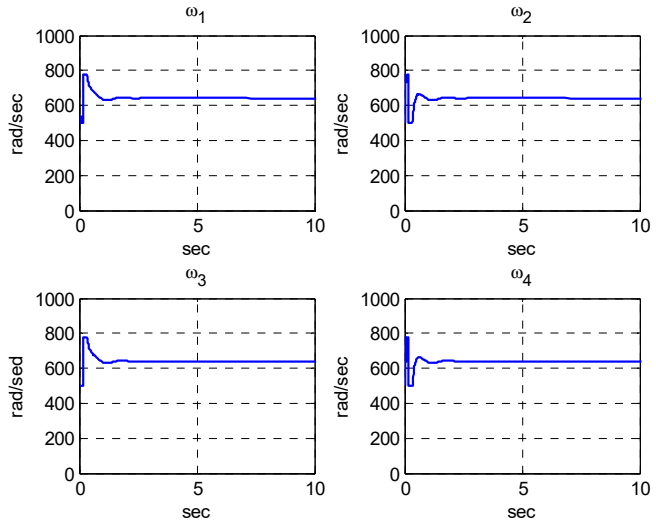

Figure 8. The rotor velocity with variable deviations.

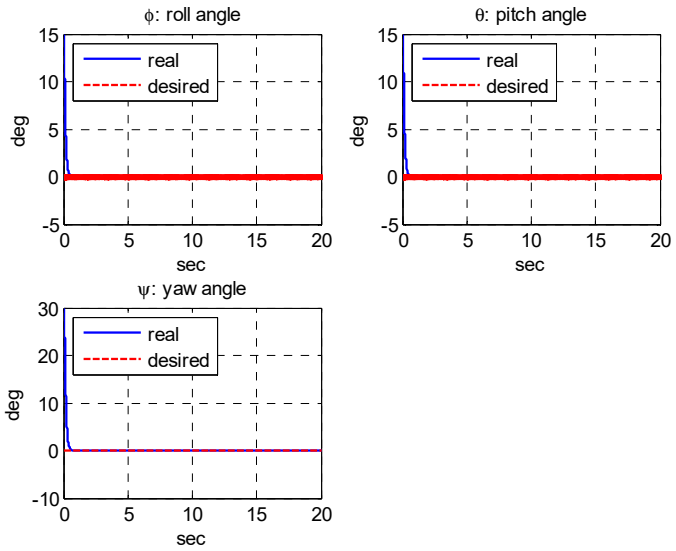

Figure 9. The attitude path with variable deviations and perturbations.

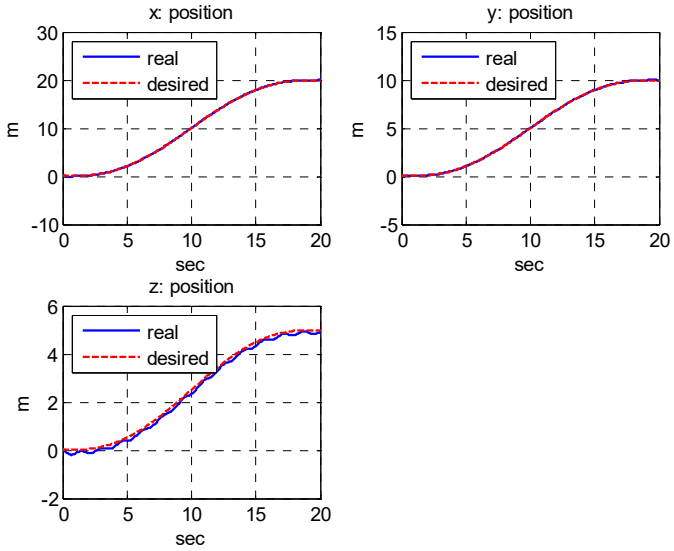

Figure 10. The position path with variable deviations and perturbations.

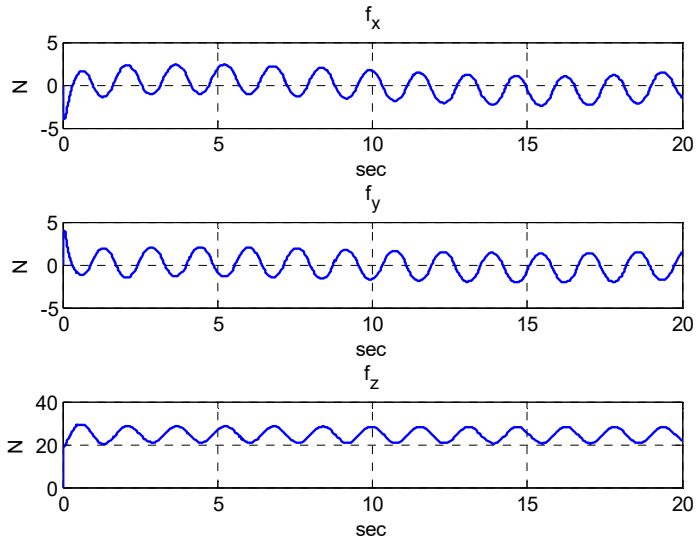

Figure 11. The propelling force with variable deviations and perturbations.

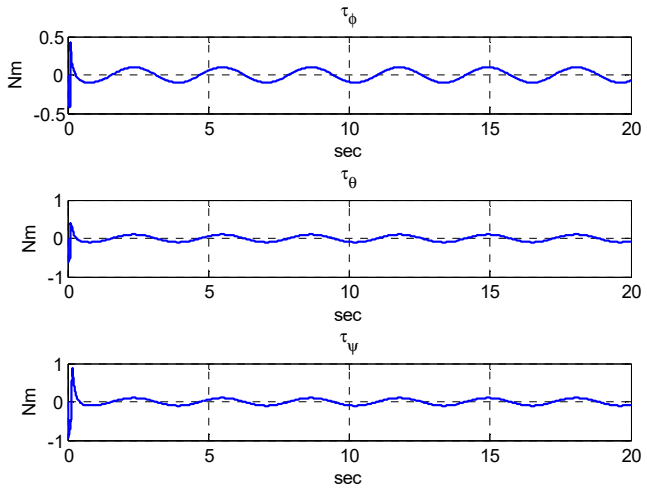

Figure 12. The turning torque with variable deviations and perturbations.

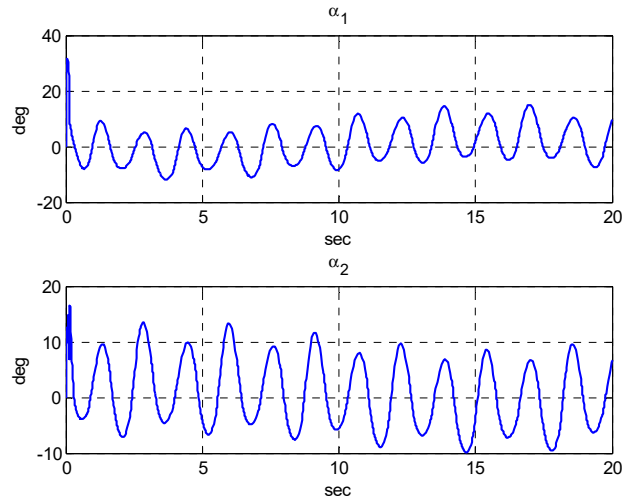

Figure 13. The tilt angle path with variable deviations and perturbations.

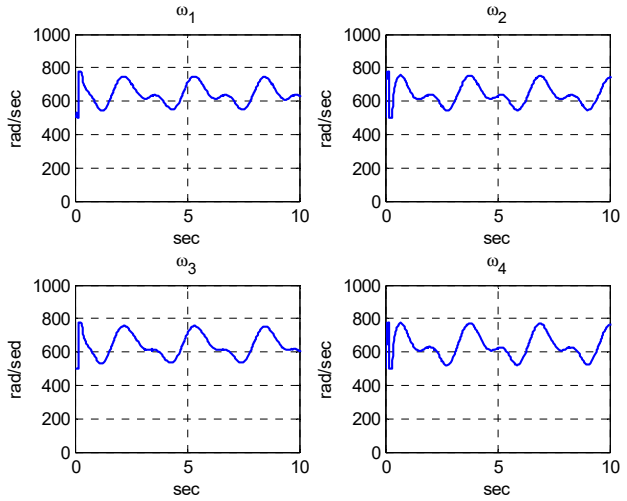

Figure 14. The rotor velocity with variable deviations and perturbations.

In summary, the numerical simulation results clearly show that the proposed SMC schemes can accomplish the goal of trajectory tracking and counter the parametric variation and external disturbances in the rotation and translation of TRQ via control allocation.

6. Conclusions

This paper presents the dynamic modeling, path following, and control allocation of a TRQ. Two types of SMC are proposed to enhance the robustness and capability: one is the first-order sliding mode for attitude following and the other is the second-order sliding mode for position following. Considering the parameter changes and external perturbation, we show the stability analysis based on the Lyapunov theory that the proposed control scheme can ensure the error dynamics' asymptotic stability for the position and attitude following. In the numerical simulation of the fully actuated mode, we demonstrated that the proposed SMC could achieve path following and attitude regulation goals in the presence of variable changes and external perturbations. The tilt-rotor quadrotor has more control degrees of freedom than the under-actuated quadrotor and, therefore, can make full use of the control redundancy to complete the simultaneous trajectory tracking and attitude control that a traditional quadrotor cannot do, and thus has a certain degree of actuator fault tolerance. In the future, we will integrate the sliding mode path following and control allocation into a fault-tolerant flight control.

Author Contributions: Conceptualization, C.-C.Y. and S.-J.W.; methodology, C.-C.Y. and S.-J.W.; software, S.-J.W.; validation, C.-C.Y. and S.-J.W.; formal analysis, C.-C.Y.; investigation, S.-J.W.; writing—original draft preparation, C.-C.Y. and S.-J.W.; writing—review and editing, C.-C.Y.; visualization, S.-J.W. All authors have read and agreed to the published version of the manuscript.

Funding: This research received no external funding.

Institutional Review Board Statement: Not applicable.

Informed Consent Statement: Not applicable.

Data Availability Statement: No new data were created or analyzed in this study. Data sharing is not applicable to this article.

Conflicts of Interest: The authors declare no conflict of interest.

Nomenclature

B	quadrotor body
P_i	propeller i
F_w	inerita world frame
F_B	body frame
F_{P_i}	ith propeller frame
R_T	transform matrix from body angular rates to Euler rates
p	position of B in F_w
q	Euler angle of B in F_w
${}^{W}R_B$	rotation matrix from F_B to F_w
${}^{B}R_{P_i}$	rotation matrix from F_{P_i} to F_B
w_i	ith propeller spinning velocity about Z_{Pi}
w_{P_i}	the angular velocity in the ith propeller frame
α_i	ith propeller tilting angle about X_{Pi}
T_{P_i}	the force in the ith propeller frame
w_B	angular velocity of B in F_B
v_B	velocity of B in F_B
τ_B	torque in F_B
τ_{P_i}	torque in F_{P_i}
τ_{di}	ith propeller air drag torque about Z_{Pi}
T_i	ith propeller thrust along Z_{Pi}
τ_{w_i}	motor torque along Z_{Pi}
m	total quadrotor mass
I_{Pi}	inertia of the ith propeller P_i
I_B	inertia of the quadcopter body B
k_f	propeller thrust coefficient
k_m	propeller drag coefficient
L	distance of F_{P_i} to F_B
g	gravity constant

References

1. Mahony, R.; Kumar, V.; Corke, P. Multirotor Aerial Vehicles: Modeling, Estimation, and Control of Quadrotor. *IEEE Robot. Autom. Mag.* **2012**, *19*, 20–32. [CrossRef]
2. Quan, Q. *Introduction to Multicopter Design and Control*; Springer: Berlin/Heidelberg, Germany, 2017.
3. Miranda-Colorado, R.; Aguilar, L.T. Robust PID control of quadrotors with power reduction analysis. *ISA Trans.* **2020**, *98*, 47–62. [CrossRef] [PubMed]
4. Gomes, L.L.; Leal, L.; Oliveira, T.R.; Cunha, J.P.V.S.; Revoredo, T.C. Unmanned Quadcopter Control Using a Motion Capture System. *IEEE Lat. Am. Trans.* **2016**, *14*, 3606–3613. [CrossRef]
5. Shankaran, V.P.; Azid, S.I.; Mehta, U.; Fagiolini, A. Improved Performance in Quadrotor Trajectory Tracking Using MIMO PI-D Control. *IEEE Access* **2022**, *10*, 110646–110660.
6. Lee, D.; Kim, H.J.; Sastry, S. Feedback Linearization vs. Adaptive SMC for a Quadrotor Helicopter. *Int. J. Control Autom. Syst.* **2009**, *7*, 419–428. [CrossRef]
7. Satici, A.C.; Poonawala, H.; Spong, M.W. Robust Optimal Control of Quadrotor UAVs. *IEEE Access* **2013**, *1*, 79–93. [CrossRef]

8. Koksal, N.; An, H.; Fidan, B. Backstepping-based adaptive control of a quadrotor UAV with guaranteed following capability. *ISA Trans.* **2020**, *105*, 98–110. [CrossRef]
9. Young-Cheol, C.; Hyo-Sung, A. Nonlinear Control of Quadrotor for Point Following: Actual Implementation and Experimental Tests. *IEEE/ASME Trans. Mechatron.* **2015**, *20*, 1179–1192.
10. Perozzi, G.; Efimov, D.; Biannic, J.-M.; Planckaert, L. Path following for a quadrotor under wind perturbations: SMC with state-dependent gains. *J. Frankl. Inst.* **2018**, *355*, 4809–4838. [CrossRef]
11. Xu, G.; Xia, Y.; Zhai, D.-H.; Ma, D. Adaptive prescribed capability terminal sliding mode attitude control for quadrotor under input saturation. *IET Control Theory Appl.* **2020**, *14*, 2473–2480. [CrossRef]
12. Besnard, L.; Shtessel, Y.B.; Landrum, B. Quadrotor vehicle control via SMCler driven by sliding mode perturbation observer. *J. Frankl. Inst.* **2012**, *349*, 658–684. [CrossRef]
13. Ricardo, J.A., Jr.; Santos, D.A.; Oliveira, T.R. Attitude Tracking Control for a Quadrotor Aerial Robot Using Adaptive Sliding Modes. In Proceedings of the XLI Ibero-Latin-American Congress on Computational Methods in Engineering (ABMEC), Foz do Iguaçu, Brazil, 16–19 November 2020.
14. Islam, S.; Liu, P.X.; El Saddik, A. Robust Control of Four-Rotor Unmanned Aerial Vehicle With Perturbation Uncertainty. *IEEE Trans. Ind. Electron.* **2015**, *62*, 1563–1571. [CrossRef]
15. Dierks, T.; Jagannathan, S. Output Feedback Control of a Quadrotor UAV Using Neural Networks. *IEEE Trans. Neural Netw.* **2010**, *21*, 50–66. [CrossRef] [PubMed]
16. Wu, H.; Ye, H.; Xue, W.; Yang, X. Improved Reinforcement Learning Using Stability Augmentation With Application to Quadrotor Attitude Control. *IEEE Access* **2022**, *10*, 67590–67604. [CrossRef]
17. Yang, S.; Xian, B. Exponential Regulation Control of a Quadrotor Unmanned Aerial Vehicle With a Suspended Payload. *IEEE Trans. Control Syst. Technol.* **2020**, *28*, 2762–2769. [CrossRef]
18. Levant, A. Principles of 2-sliding mode design. *Automatica* **2007**, *43*, 576–586. [CrossRef]
19. Levant, A. Sliding order and sliding accuracy in SMC. *Int. J. Control* **1993**, *58*, 1247–1263. [CrossRef]
20. Utkin, V.I.; Poznyak, A.S. Adaptive SMC with application to super-twist algorithm: Equivalent control method. *Automatica* **2013**, *49*, 39–47. [CrossRef]
21. Moreno, A.; Osorio, M. Strict Lyapunov functions for the super-twisting algorithm. *IEEE Trans. Autom. Control* **2012**, *57*, 1035–1040. [CrossRef]
22. Pico, J.; Pico-Marco, E.; Vignoni, A.; De Battista, H. Stability preserving maps for finite-time convergence: Super-twisting sliding-mode algorithm. *Automatica* **2013**, *49*, 534–539. [CrossRef]
23. Utkin, V. On convergence time and perturbation rejection of super-twisting control. *IEEE Trans. Autom. Control* **2013**, *58*, 2013–2017. [CrossRef]
24. Mokhtari, A.; Benallegue, A.; Orlov, Y. Exact linearization and sliding mode observer for a quadrotor unmanned aerial vehicle. *Int. J. Robot. Autom.* **2006**, *21*, 39–49. [CrossRef]
25. Beballegue, A.; Mokhtari, A.; Fridman, L. High-order sliding-mode observer for a quadrotor UAV. *Int. J. Robust Nonlinear Control* **2008**, *18*, 427–440. [CrossRef]
26. Bauersfeld, L.; Spannagl, L.; Ducard, G.J.J.; Onder, C.H. MPC Flight Control for a Tilt-Rotor VTOL Aircraft. *IEEE Trans. Aerosp. Electron. Syst.* **2021**, *57*, 2395–2409. [CrossRef]
27. Ryll, M.; Bülthoff, H.H.; Giordano, P.R. A Novel Overactuated Quadrotor UnmannedAerial Vehicle: Modeling, Control, and Experimental Validation. *IEEE Trans. Control Syst. Technol.* **2015**, *23*, 540–556. [CrossRef]
28. Hua, M.-D.; Hamel, T.; Morin, P.; Samson, C. Control of VTOL vehicles with thrust-tilting augmentation. *Automatica* **2015**, *52*, 1–7. [CrossRef]
29. Rashad, R.; Goerres, J.; Aarts, R.; Engelen, J.B.C.; Stramigioli, S. Fully Actuated Multirotor UAVs: A Literature Review. *IEEE Robot. Autom. Mag.* **2020**, *27*, 97–107. [CrossRef]
30. Zheng, P.; Tan, X.; Kocer, B.B.; Yang, E.; Kovac, M. TiltDrone: A Fully-Actuated Tilting Quadrotor Platform. *IEEE Robot. Autom. Lett.* **2020**, *5*, 6845–6852. [CrossRef]
31. Willis, J.; Johnson, J.; Beard, R.W. State-Dependent LQR Control for a Tilt-Rotor UAV. In Proceedings of the 2020 American Control Conference (ACC), Denver, CO, USA, 1–3 July 2020; pp. 4175–4181.